On the nature of majority and minority traps in β-Ga_2O_3: A review

Labed Madani [1,*], Sengouga Nouredine [2], Chowdam Venkata Prasad [1], Henini Mohamed [3] and You Seung Rim [1,4,*]

[1]*Department of Intelligent Mechatronics Engineering and Convergence Engineering for Intelligent Drone, Sejong University, Seoul, 05006, Republic of Korea.*

[2]*Laboratory of Semiconducting and Metallic Materials (LMSM), University of Biskra, 07000, Algeria.*

[3]*School of Physics and Astronomy, University of Nottingham, Nottingham NG7 2RD, UK.*

[4] *Department of Semiconductor Systems Engineering, Sejong University, Seoul, 05006, Republic of Korea.*

* Corresponding authors:

E-mail: madani@sejong.ac.kr (L.M) youseung@sejong.ac.kr (Y.S. Rim).

Abstract

In the last decade, researchers and commercial companies have paid great attention to ultrawide bandgap semiconductors especially gallium oxide (Ga_2O_3). Ga_2O_3 has very interesting properties such as a bandgap higher than 4.8 eV, high electrical breakdown field and easy to control the doping density. For example, vacancies and impurities play an important role in controlling the n-type conductivity of this material and hence improving the device performance. This review paper discusses mostly the point defects in Ga_2O_3 and the sources of majority and minority deep levels (traps) in Ga_2O_3 characterized using different methods such as deep level transient spectroscopy (DLTS), optical DLTS (ODLTS), deep level optical spectroscopy (DLOS) and other techniques. Majority traps such as E1, E2*, E2 and E3 with energies of about 0.56, 0.75, 0.79 and 1.05 eV below the conduction band maximum (CBM), respectively, are the most observed in Ga_2O_3. These

traps are mostly related to impurities such as iron (Fe), silicon (Si), titanium (Ti) and other impurities, or alternatively to gallium or oxygen vacancies. Minorities traps H1, H2 and H3 with energies of about 0.2, 0.3 and 1.3 eV, respectively, above the valence band maximum (VBM) are the most known defects that are related to vacancies. These minorities traps are usually extracted using optical techniques because of the very low hole density in Ga_2O_3.

Keywords: Ga_2O_3, review, traps, formation energy, majority, minority, DLTS, ODLTS, ODLS, TL.

1. Introduction:

Over the past few years, there has been a renaissance in the study of beta-phase gallium oxide (β-Ga_2O_3). The ultra-wide bandgap of 4.8 eV, the widely tunable n-type conductivity ranging between 10^{16} and 10^{19} cm^{-3}, the high theoretical breakdown field of 8 MV/cm, the high electron saturation velocity of 2×10^7 cm/s, the large Baliga's Figure of Merit (BFOM), and the availability of large and high-quality single-crystal substrates are some of the characteristics that have sparked interest in this material [1]. Deep ultraviolet (DUV) LEDs and high-power devices operating in severe environments, such as ionizing radiation in space, are made possible by the use of ultra-wide bandgap (UWBG) semiconductors. The β-Ga_2O_3 crystal structure belongs to the C2/m space group and has the following lattice constants: a = 1.22 nm, b = 0.303 nm, c = 0.580 nm, and angle β = 103.8° [1,2]. For large-size single crystals, melt growth procedures such edge-defined film-fed growth (EFG)[3], Czochralski method (CZ)[4], and floating-zone (FZ) [5] have been utilized successfully. Conductive β-Ga_2O_3 substrates are produced by Si [6] and Sn [4,7] doping with a carrier concentration in excess of 10^{18} cm^{-3}, which is necessary to produce vertical devices with high breakdown voltage. Higher free carrier concentration is produced by a higher shallow dopant concentration, but the mobility is decreased by impurity scattering[8]. Particularly

for strongly doped Ga_2O_3, free carrier absorption occurs, and the plasma frequency shifts to shorter wavelengths with a greater free carrier concentration [9]. In addition to the well-known reduction of minority carrier lifetimes through non-radiative recombination, deep defect states also play a crucial role in the creation of semi-insulating materials in the case of Iron (Fe) doped β-Ga_2O_3[10].

In last year, there is great interest of studying traps in β-Ga_2O_3. This can be seen by the high increasing in the number of the published research papers about traps in β-Ga_2O_3 using different techniques such as deep-level transient spectroscopy (DLTS), optical deep-level transient spectroscopy (ODLTS) and deep-level optical spectroscopy (DLOS) and other techniques.

In general, β-Ga_2O_3 deep traps can be classified into two types, majority and minority traps. This classification is either based on its capability to capture an electron (majority trap) or a hole (minority trap) which is clearly manifested in the capture cross-section rate value or depends on how close to the valence band maximum (VBM) and/or conduction band minimum (CBM).

DLTS, ODLTS and DLOS have been widely used up in order to examine the basic characteristics of deep-level defects in β-Ga_2O_3. Recent research on deep electron traps in n-type β-Ga_2O_3 Schottky barrier diodes (SBDs) has enabled mapping of the upper half of the bandgap and revealed the presence of four deep electron traps with activation energy values near E_c-0.6 eV (E1), E_c-0.79 eV (E2), E_c-0.75 eV (E2*) and E_c-1 eV (E3) [11–15].

DLTS is based on measuring the transient capacitance arising from the depletion region at different temperatures and voltages. This transient capacitance is very sensitive to capture and emission processes of majority and minority charge carrier traps. However, in ODLTS and DLOS, optical illumination is used to activate the carriers located in traps, and they are mostly used to detect minority traps with very deep energies. When exposed to high energy particles, the concentrations of E2* and E3 centers were found to significantly increase[14]. These centers were

also thought to be involved in conductivity compensation. The sites of these levels resemble the locations of donors related oxygen vacancies as predicted by theory [16], and in strong electric fields, the activation energies of these centers are reduced. This is consistent with these levels being deep donors and not participating in n-type material compensation[17]. In addition, a correlation between changes in such electron trap concentration and a reduction in the diffusion lengths of charge carriers has also been reported [15].

The majority of the DLTS measurements were performed using β-Ga_2O_3 SBDs, which are effectively majority carrier devices. As a result, traditional thermal excitation is unable to access the whole defect spectrum across wide bandgap semiconductors. Only majority carrier traps with energy levels less than 1 eV below the CBM have been observed [18,19]. Other techniques such as thermoluminescence (TL) [20], surface photovoltage spectroscopy (SPS) [21,22] and depth-resolved cathodoluminescence spectroscopy(DRCL) [21] are used for traps extraction. However, In order to detect minority traps near VBM of β-Ga_2O_3, DLOS and ODLTS were employed [25]. In these methods optical excitation with photon energies that were slightly above the material bandgap are used. The time constants for optical emission are slower than those for a normal thermal transient, which makes it difficult to determine the precise concentration of each trapping level and distinguish between states for Ga_2O_3 with numerous sub-gap states [26]. In addition to the optical methods, conventional DLTS can be used but in a heterojunction consisting of n-type Ga_2O_3 and highly doped p^+-type layer such NiO with high hole density.

In this review, the electronic structures of defects and their formation energies will be discussed in detail in terms of first-principle calculations. In addition, majority and minority traps extracted using DLTS, TL, PL, ODLTS and DLOS techniques will be presented. Furthermore, particular attention is focused on the famous majority traps E1, E2, $E2^*$ and E3 and H1, H2 and H3 minority

traps. Moreover, this review describes DLTS, ODLTD, DLOS, TL and PL techniques for the readers.

2. Ga_2O_3 Polymorphs and Crystal structures:

There are several polymorphs of Ga_2O_3, which were studied in detail experimentally and theoretically by many researchers including Roy at al.[27], Zinkevich and Aldinger[28], Penner et al.[29], Playford et al. [30], Yoshioka et al. [31], Bosi et al. [32], Delgado et al. [33] and Cora et al.[34] and others. Although as many as six polymorphs (α, β, γ, δ, ε, and κ) having different crystallographic systems has been reported for Ga_2O_3 as presented in **Table 1,** there are likely only four polymorphs: α, β, γ, and (δ/ ε/ κ). The δ-phase could be a mixture of β and ε phases, according to Playford et al. [30], while the ε phase could resemble the κ phase due to rotation grains formed on sapphire, as shown by Cora et al. [34].

However, β phase is the most thermodynamically stable and can be grown directly from melt. **Figure 1** shows monoclinic β-Ga_2O_3 which has a C2/m symmetry with four formula units in the conventional unit cell with 20 atoms (Ga^{+3} and O^{-2}) characterized by four lattice parameters (a, b, c and β) [36] given in **Table 1**. In addition, the melting point of β-Ga_2O_3 is about of 1793 °C. The formation energy of the polymorphs have the following order $\beta < \varepsilon < \alpha < \delta < \gamma$ [31].

Most bulk and thin film β-Ga_2O_3 available today have n-type conductivity because of the unintentional presence of silicon, hydrogen and other impurities which act as shallow donors in both interstitial and substituted Ga atoms in the crystal structure[16,39]. In addition, different dopants, such as Si[40], Mg[41], Ge[42], Sn[43], Nb[44], Ta[45], Fe[46], and Cr[47], are used to

increase n-type conductivity of β-Ga_2O_3 as will be discussed in detail in this review. For p-type β-Ga_2O_3, there are many attempts to improve its stability [48–50], but this material suffers from the very low hole mobility which is related to the very high effective hole mass because of the very flat top of valence band[16] as shown in **Figure 2.**

III. Point defects in β-Ga_2O_3:

Defects in general affect the electrical, optical, mechanical and electronic properties of β-Ga_2O_3. In addition to point defects and extended defects, defects can be categorized considering their location in the crystal, as bulk or surface defects. In this review paper, only point defects and their effect on majority and minority traps in β-Ga_2O_3 will be investigated.

A point defect is an imperfection that occurs at a specific location in the crystal. These point defects can be vacancies such as oxygen and gallium vacancies (intrinsic defects) or impurities, which replace Ga or oxygen atoms in β-Ga_2O_3 crystal structure (extrinsic defects).

Usually, the effect of oxygen vacancies (V_O) and their role on β-Ga_2O_3 properties are studied theoretically using density functional theory (DFT)[16,51], which is based on the electron density distribution and positions of the nuclei. Binet et al.[52] found that n-type conductivity of β-Ga_2O_3 is due to oxygen vacancies which form shallow donors with an ionization energy of about 0.04 eV. However, many studies reported that oxygen vacancies form deep levels rather than shallow donor levels. For example, Varley et al.[16], using hybrid functional method, found that oxygen vacancies in which O (I) and O (II) are threefold coordinated, while O (III) is fourfold coordinated as shown in **Figure 3,** have formation energies of 3.31 eV, 2.70 eV and 3.57 eV, respectively. Therefore, oxygen vacancies form deep donor levels and cannot explain the unintentional n-type conductivity of β-Ga_2O_3. These formation energies are close to those published by Dong et.al[53]

which are 3.2 eV, 3.7 eV and 3.9 eV for O (I), O (II) and O (III), respectively. Furthermore, gallium vacancies (V_{Ga}) are expected to be point defects in β-Ga_2O_3 since Ga has doubly ionized (V_{Ga}^{-2}) and singly ionized (V_{Ga}^{-1}) gallium vacancies as shown in **Figure 3**, with V_{Ga}^{-1} having a lower formation energy than V_{Ga}^{-2}[54,55] which form deep acceptor levels[56].

The second type of point defects are extrinsic defects, which form shallow or deep traps. Si atom can replace Ga (I)[16] or sometimes Ga (II)[58]. The formation energies for Si in Ga (I) vacancy for O-poor condition is lower than for O-rich condition [59]. This indicates that Si-doped β-Ga_2O_3 can be formed easily under O-poor condition. Sn atoms also form shallow levels with a formation energy lower than the formation energy of Si atoms for O-rich condition and higher for O-poor condition[16,59] as shown in **Figure 4**.

Furthermore, Chlorine (Cl) atoms, which prefer O (I) sites, have a formation energy higher than that for Si and Sn for both O-rich and O-poor conditions as shown in **Figure 4**. Varley et al.[16] and Sun et al.[60] suggested that Cl atoms, which form shallow levels, have a strong effect on β-Ga_2O_3 n-type conductivity.

According to Ingebrigtsen et al. [61], Iron atoms (Fe) can be incorporated in both tetrahedral sites (Ga(I)) or octahedral sites (Ga(II) with a low formation energy for O-rich condition as shown in **Figure 5.** Both cases can form trap levels of about 0.61 and 0.59 eV below the conduction band. However, according to electron paramagnetic resonance spectroscopy (EPR) study, Fe^{+2} has not been observed in contrast to Fe^{+3} which is detected in bulk β-Ga_2O_3.

3. Trap states in Ga_2O_3:

As mentioned in the introduction, deep traps in Ga_2O_3 can be classified into two types, namely majority and minority traps. Although optical and thermal methods, including thermally stimulated luminescence (TSL), photoluminescence (PL) and surface photovoltage spectroscopy, can be used for deep trap detection, DLTS (deep level transient spectroscopy) and its variants are the mostly employed techniques in this respect.

Conventional DLTS technique is based on measuring the transient capacitance arising from the depletion region of a SBD or a heterojunction. The transient capacitance is given by[62]:

$$C(t) = A\frac{\varepsilon}{d} = A\sqrt{\frac{q\varepsilon(N_d - N_t(t))}{2(V_{bi} - V)}} \quad (1)$$

where ε, d, A, $N_d - N_t(t)$, V_{bi} and V are the dielectric constant of semiconductor, depletion region width, contact area between the metal and the semiconductor, the difference between doping density and traps transient density, built-in potential and applied bias, respectively.

Furthermore, bias pulses are periodically applied at a fixed repetition frequency to change the occupancy of the traps. Firstly, the device is subjected to a reverse bias (V_R) to empty the traps above the Fermi level and increasing the depletion region as shown in **Figure 6 (a)**. Then, as shown in **Figure 6 (b)**, a filling pulse (V_P) is applied with fixed pulse width, causing the depletion region width to decrease and the traps present in the depletion region to be filled with carriers. Finally, a reverse bias is re-applied and the depletion region increases again and the filled traps start to emit carriers as shown in **Figure 6 (c)** resulting in a change of capacitance with time because of the emission and capture processes. Since the depletion region is highly ionized, the capture process can be ignored with the assumption of electrons emission domination ($e_n \gg e_p, C_n, C_p$). The transient capacitance is usually, for $N_t \leq N_d/10$, given by[63]:

$$C(t) \approx C_\infty \left[1 - \frac{N_t}{2N_d}\exp\left(-e_n t\right)\right] \quad (2)$$

where C_∞ and e_n are the maximum reverse bias capacitance and electron emission rate, respectively.

Since the emission process is thermally stimulated, the output signal of the change of the transient capacitance ($\Delta C(t)$) is measured between two times t_1 and t_2 (boxcar method) at different temperatures (T). Using previous equation, the DLTS output signal as function of T, S (T) given by[63]:

$$S(T) = C(t_2) - C(t_1) = \Delta C_0 \left[\exp\left(-\frac{t_2}{\tau}\right) - \exp\left(-\frac{t_1}{\tau}\right)\right] \quad (3)$$

where τ is the inverse of the electron emission rate ($\tau = 1/e_n$).

τ can be evaluated from the maximum signal S(T) $\left(\frac{\partial S(T)}{\partial \tau} = 0\right)$ as:

$$\tau = \frac{t_1 - t_2}{\ln(t_1/t_2)} \quad (4)$$

ΔC_0 is the change in the capacitance at t=0, which is given by[63]:

$$\Delta C_0 \approx \frac{C_\infty N_t}{2N_d} \quad (5)$$

The DLTS signal (S(T)) is calculated at different temperatures as shown in **Figure 7 (a)** for traps in a β-Ga_2O_3 SBD scanned from 200 K to 350 K with a reverse bias V_R=-8 V, a filling pulse height of about V_P = -0.1 V and filling pulse width t_f =1 ms. Consequently, the obtained Arrhenius plots are shown in **Figure 7 (b)**. Trap level activation energy (E_t) and capture cross-section (σ_n) can be extracted from the slope and intercept of the Arrhenius plots, respectively, as indicated in **Figure 7(b)**. In DLTS, the trap concentration can be determined from the change in the capacitance at t=0 s in equation (**5**). It is worth mentioning that the DLTS signal sign of minority traps is opposite to majority traps.

Conventional DLTS is a thermal scanning technique where the temperature of the diode is changed continuously during the acquisition of the capacitance transient which may lead to the formation of broad DLTS spectrum peaks [64], thus affecting the accuracy of the extracted traps characteristics. In addition, the resolution of the time constant is also problematic as DLTS cannot distinguish amongst closely spaced defects with comparable emission rates. To overcome these limitations, Laplace DLTS (LDLTS) is used to extract the emission rate (e_n) from the Laplace Transform of the capacitance transient at a fixed temperature, which makes the LDLTS to be an isothermal technique[64]. **Figures 8 (a)** and **(b)** show the extracted traps levels using DLTS and LDLTS.

Furthermore, there are other technique can be used for deep, shallow and minority traps extraction such as thermoluminescence (TL), which is a powerful technique based on light emission under the effect of thermal stimulation after irradiation the sample. After irradiation using Xenon lamp, electron excited from valence band to conduction band. These electrons can be taping by non-radiative centers. Then, because of the effect of thermal stimulation and retrapping of these electrons can be occupy a radiative recombination the full process is summarized in **Figure 9**. From the emitted energy and using mathematical model for TL, which can be constructed from the Arrhenius equation and then trap energy level can be extracted.

For very deep traps or minority traps (hole traps) in β-Ga_2O_3, DLTS and LDLTS require very high temperatures. Deep level optical spectroscopy (DLOS) or optical deep level transient spectroscopy (ODLT) techniques are used instead where an optical excitation signal of the deep levels replaces the electrical one, which is used in DLTS and Laplace DLTS. In ODLTS, a monochromatic illumination is used for optical excitation with temperature scanning. However, in DLOS, a different illumination energy is used at a fixed temperature. For example, for β-Ga_2O_3 the optical excitation energy must be higher than the β-Ga_2O_3 bandgap. Usually Xe- lamps are used which provide photons over a wide range of energies (1.2 eV to 5 eV)[13]. In addition, there are other techniques such as photoluminescence (PL), depth-resolved cathodoluminescence spectroscopy (DRCL) and surface photovoltage spectroscopy (SPS) techniques, which are used mostly for very deep trap extraction and minority traps, as we will discuss.

3.1. Majority traps (electron traps)

3.1.1. E2 trap level

Majority traps in β-Ga_2O_3 were first reported by Irmscher et al.[12] for different crystal structures with V_R= -10 V (except the samples #5 and #7 biased at V_R= -4 V), V_P=0 V and $t_p = 100$ µs. It was found that, in most cases, a trap level lying at ~0.78 eV below CBM is dominant and it was labelled as E2 with density higher than 1×10^{16} cm^{-3} [12,65]. This trap level extracted in most β-Ga_2O_3 traps analysis works based on DLTS [12,19,61,65,67] or TL[66,68] and not detected by ODLTS or DLOS because these techniques are used mostly for very deep traps levels as we will discuss. In most cases, this trap level related to impurities such as Fe^{+3} and Co^{+2} which prefer to substitute both Ga (II) or Ga(I) sites [12,61,65,67] as we discussed before.

Zimmermann et al.[69] used steady-state photo-capacitance(SSPC) method with first-principles calculations confirmed the trap formed trap level for each case. For $Fe_{Ga\ (I)}$, the formed trap level

is 0.66 eV; however, for $Fe_{Ga\ (II)}$ the formed trap level is deeper with energy level 0.79 eV. This trap level its important lies in reducing β-Ga_2O_3 conductivity and forms semi-insulating β-Ga_2O_3 layer by compensating and capturing free electrons in β-Ga_2O_3 layer, for example Ueda et al.[70] found an increase in resistivity with increasing Fe concentration in β-Ga_2O_3. This semi-insulating layer is used for developing a high performance metal-oxide-semiconductor field effect transistor (MOSFET)[71].

Furthermore, for understanding the source of this trap and other traps, β-Ga_2O_3 analyzed at different conditions. Polyakov et al. [72] analyzed β-Ga_2O_3 exposed to Ar plasma revealed that E2 is not detected, which maybe due to the high density of other surface traps. However, a very close trap level (Ec-0.8 eV, where E_c is the bottom of the conduction band) was detected near the surface and in the bulk. After Ar plasma exposer, a high increasing in Ec-0.8 density near the surface of β-Ga_2O_3 as shown in **Figure 10**.

In other work, Polyakov et al.[14] studied the effect of 10 MeV proton irradiated on β-Ga_2O_3 films grown by Hydride Vapor Phase Epitaxy (HVPE). They found that, E2 trap density increased from 4.6×10^{13} cm^{-3} to 3.2×10^{14} cm^{-3} after irradiation. The increasing in E2 trap level density her and E_c-0.8 as presented in **Figure 10**, supports Ga vacancy source of this trap level especially Ar plasma and proton irradiation increase Ga vacancy density in the surface of β-Ga_2O_3[11,21,24].

However, Ingebrigtsen et al. [11] analyzed single crystal β-Ga_2O_3 irradiated by Proton with dose 6×10^{14} cm^{-2}. As shown in **Figure 11**, after irradiation E2 trap level is not affected in contrast to the other trap. This results agree with the result obtained by Zimmermann et al.[73] they studied the effect of helium and hydrogen implementation and E2 trap level not affected.

Using TL technique, Luchechko et al.[68] analyzed the source of each trap level for Cr^{+3} and Mg^{+2} doped β-Ga_2O_3 at different concentrations. Cr^{+3} and Mg^{+2} atoms prefer Ga sites in β-Ga_2O_3 [74,75]. The extracted traps levels for both cases were E_C-0.55 eV~E1, E_C-0.62 eV, E_C-0.7 eV~$E2^*$, E_C-0.78 eV~E2, E_C-0.94 eV and E_C-1.1 eV. After doping with Cr^{+3} and Mg^{+2} atoms, E_C-0.55 eV and $E2^*$ trap levels intensity increased substantially in comparison with the unintentionally doped sample as shown in **Figure 12** in contrast to E2, which indicates that the source of E2 trap level not Cr^{+3} and Mg^{+2} atoms.

In order to resolve this controversy, Ingebrigtsen et al. [61] used a combination of DLTS and secondary in mass spectroscopy (SIMS) to confirm the origin of this trap level. As shown in **Figure 13**, Si atoms in β-Ga_2O_3 show a weak dependence with E2 level, which confirms that Si forms a shallow level. This is in contrast to Fe atoms, which have a linear dependence with E2 concentration. This indicates that the source of this trap level is related to Fe^{+3}.

3.1.2. E1 trap level

E1 is another dominating trap, with an energy level 0.4-0.66 eV below CBM. This trap is related mainly to simple point defects in β-Ga_2O_3 such as Cr^{3+}, Fe^{+2} or Co^{+3} impurities [68]. According to Polyakov et. al[76], three configurations of this trap are expected as a source, either $Si_{Ga(I)}$-H or $Si_{Ga(II)}$-H complexes, Si residual major impurity or Sn impurity with less probability. These impurities are possibly incorporated during the growth process [65,77,78]. Most of these traps in the range 0.4-0.66 eV below CBM are labelled E1. According to LDLTS analysis, this trap level is located at Ec-0.56 eV as shown in the inset of **Figure 8 (b)** [65]. The impurity source of this trap can be confirmed from the effect of Ar plasma exposer and proton irradiation. As shown in

Figure 10 and **11,** we can observe this trap is not affected by Ar plasma and proton irradiation. This indicates this trap level related to impurities like Cr^{3+}, Fe^{+2} or Co^{+3}.

3.1.3. $E2^*$ trap level

Another trap which is very close to E2 with energy around E_c-0.75 or closer are usually referred to as $E2^*$ with a concentration of about ~10^{14} cm^{-3}. Most of these traps are associated with intrinsic native defects such as oxygen vacancies[13,24,61]. As sown in **Figure 11,** after exposed the surface of β-Ga_2O_3 to proton, $E2^*$ intensity was increased. This explained by the increasing of vacancy in the surface of β-Ga_2O_3. So, this trap level can be related to native defects such as oxygen vacancies. However, Zimmermann et al.[73] studied the effect of hydrogen and helium implementation and they expected this trap is related to a complex defect and Ga_O antisites in β-Ga_2O_3, they mentioned that hydrogen atoms can passivate $E2^*$ trap level. However, as shown in **Figure 12** after doping with 0.1%Mg^{2+} a new trap level with energy E_c-0.7 formed which is very close to $E2^*$ trap level and its intensity increased more after co-doping with 0.05% Cr^{3+}, 0.1% Mg^{2+}. The origin of this trap in this work maybe related to Cr^{+3} atoms. From this work, in contrast to other works, the impurity source of this trap can be explained maybe by the shifting of E1 trap level from Ec-0.55 to 0.7 because as we discussed before E1 trap originated from impurities like Cr^{3+}, Fe^{+2} or Co^{+3}. So, the shifting maybe related to the effect of charges like oxygen vacancy (V_o) which will effect on the electron trapping, this will influence the trap energy shifting further from CBM, from E_C-0.55 eV to E_c-0.7 eV.

3.1.4. E3 trap level

In addition, another important electron trap is the Ec-1.05 eV or near trap energy level, which is labelled E3. This trap level is obtained in most published work and it is related to several source. Some works related it to intrinsic traps such as vacancies and other related this trap level to impurities such as Fe and titanium (Ti). The first expected source, as shown in **Figure 10**, this trap level concentration highly increased from 5×10^{13} cm^{-3} to 8.9×10^{15} cm^{-3} after Ar plasma exposer. This means that Ar plasma treatment increases the vacancies density, which leads to an increase of E3 density. In contrast to proton irradiation, E3 trap level not affected as shown in **Figure 11**. Furthermore, according to Irmscher et al. [79] Fe^{+3} and Co^{+2} impurities are expected as sources of this trap level.

A very close trap level, Ec-0.95 eV, was observed by Zimmermann et al.[65] using DLTS analysis and SIMS. It was related to titanium (Ti) atoms that substitute Ga (II) in β-Ga_2O_3 as shown in **Figure 14,** which presents DLTS spectra and comparison between the titanium concentration obtained from SIMS measurements and E3 concentration.

Furthermore, Islam et al. [66] studied the effect of doping β-Ga_2O_3 used TL for analyzing Fe-doped β-Ga_2O_3 and compared with undoped β-Ga_2O_3, For Fe-doped sample, a trap with energy level 1.262 eV was observed in contrast to undoped. So, for this trap level, tow sources are expected, one related to vacancies in β-Ga_2O_3 and the other is related to impurities such as Fe and Ti. For this, we expected that, there more than two close traps levels each one has a source and because of the difficulty to detect very close traps level, for each case the highest concentration is detected.

3.1.5. Other very deep levels

Traps with a very deep energy can be detected using different optical techniques such as deep level optical spectroscopy (DLOS), Deep level optical spectroscopy (DLOS), Photoluminescence (PL), thermoluminescence (TL), surface photovoltage spectroscopy (SPS) and depth-resolved cathodoluminescence spectroscopy (DRCL) techniques. Firstly, traps related to Ga vacancy (V_{Ga}) such as 2.16 eV (E4) and 3 eV (E5) which are observed by many researchers using DLOS[13,23,24], DRCL[21], SPS [21,22] and TL[20]. Most of the work related these traps levels to Ga vacancy. The source of these trap level confirmed by β-Ga_2O_3 surface irradiation and Ar plasma exposer. Firstly, GaO el.[21] studied the effect of neutron irradiation on the surface of β-Ga_2O_3 at different energy and they observed that these two traps the normalized intensity highly increased after irradiation at different energies as shown in **Figure 15 (a)** and **(b)** and the neutron irradiation mostly effect on Ga vacancy[80]. Therefore, they related this trap level to Ga vacancy (V_{Ga}). In addition, this confirmed by Polyakov et al. [24] after Ar plasma exposer of the surface of β-Ga_2O_3, new traps levels with energies 2.3 and 3.1 were detected in the surface of β-Ga_2O_3 in contrast to the bulk as shown in **Figure 10**.

3.2. Minority traps:

Using conventional DLTS, minority traps cannot be detected because of the very low hole density and low hole mobility in β-Ga_2O_3. Using ODLTS, Polyakov et al. [81] observed a minority trap with an energy level 1.3-1.4 eV above VBM. A 365 nm LED was used for the optical excitation at a temperature of about 430 K as shown in **Figure 16**. This trap is related to gallium vacancy[81]. However, this trap level is much lower than that predicted by hybride functional theory by Varley el al.[82] which is of about 0.53 eV above VBM.

Farzana et al.[25] and Zhang et al.[13] have found a very close level to the theoretical energy value of about 4.37 eV below CBM or ~0.5 eV above VBM (β-Ga_2O_3 bandgap of about ~4.85 eV) with a concentration of ~10^{16} cm^{-3} in a β-Ga_2O_3 layer grown by plasma-assisted molecular beam epitaxy using DLOS as shown in **Figure 17**. This trap level was related to oxygen and gallium vacancies [25]. Furthermore, it is related to the transition of holes from the polaronic self-trapped hole (STH) state which is at the origin of the unstable p-type conductivity and poor hole mobility drawbacks of β-Ga_2O_3[82].

Other intrinsic hole traps with energy levels near VBM, namely 0.2-0.25 eV and 0.3-0.4 eV, are referred to as H1 and H2, respectively, as shown by the ODLTS Arrhenius plots in **Figure 18**.

One of the proposed solutions to detecting minority traps in β-Ga_2O_3 using conventional DLTS is by forming a heterojunction with a highly doped p^+-type layer. Wang et al.[83] deposited highly doped p^+-NiO layer to increase hole injection to β-Ga_2O_3 by trap assisted tunneling process. For a comparable SBD, a majority trap with an energy level at E_c-0.79 eV was revealed but after the deposition of p^+-NiO, a new minority bulk trap was detected with an energy level of 0.14 eV above VBM at different frequencies and pulse time. This trap or closer traps are referred to as H3.

4. Summary:

Future developments and applications of β-Ga_2O_3 depend mostly on how much is known about the properties of this material. Among these properties, are electronic properties and traps levels in β-Ga_2O_3. In general, traps are classified into two types, majority and minority traps. In β-Ga_2O_3, majority traps or electron traps which can capture electrons are close to the conduction band and have high electron capture cross sections. Using different techniques such as DLTS, ODLTS, ODLT and other techniques, E2 trap level is usually dominant and is related in most case to Fe^{+3} or Co^{+2} impurities in Ga sites. The other trap is E1 with an energy level of about 0.4-0.66 eV below CBM which is related to Cr^{3+} impurity and $Si_{Ga(I)}$-H or $Si_{Ga(II)}$-H complexes inserted during the deposition. Another important trap, namely $E2^{*}$, is associated with native defects such as oxygen and gallium vacancies. For E3 trap, there are two possible sources: (i) impurities atoms such as Fe^{+3} and Co^{+2} or (ii) gallium vacancies. In contrast to majority traps, minority traps are close to the valence band with high capture cross sections for holes. These minority traps or hole traps are detected using only optical techniques or by forming a heterojunction with highly doped p-type layer. Three minority traps are detected, namely H1, H2 and H3 traps which are related to gallium vacancy.

Acknowledgments:

This work was supported by the National Research Foundation of Korea (NRF) grant funded by the Korea government (MSIT) (No. 2020R1A2C1013693) and the Technology Innovation Program - (20016102, Development of 1.2kV Gallium oxide power semiconductor devices technology and RS-2022-00144027, Development of 1.2kV-class low-loss gallium oxide transistor) by the Ministry of Trade, Industry, and Energy (MOTIE, Korea).

References:

[1] H.W. Xue, Q.M. He, G.Z. Jian, S.B. Long, T. Pang, M. Liu, An Overview of the Ultrawide Bandgap Ga2O3 Semiconductor-Based Schottky Barrier Diode for Power Electronics Application, Nanoscale Res. Lett. 13 (2018) 1–13. https://doi.org/10.1186/s11671-018-2712-1.

[2] S.J. Pearton, J. Yang, P.H. Cary, F. Ren, J. Kim, M.J. Tadjer, M.A. Mastro, A review of Ga 2 O 3 materials, processing, and devices, Appl. Phys. Rev. 5 (2018) 011301. https://doi.org/10.1063/1.5006941.

[3] A. Kuramata, K. Koshi, S. Watanabe, Y. Yamaoka, T. Masui, S. Yamakoshi, High-quality β-Ga2O3 single crystals grown by edge-defined film-fed growth, Jpn. J. Appl. Phys. 55 (2016) 1202A2. https://doi.org/10.7567/JJAP.55.1202A2.

[4] Z. Galazka, K. Irmscher, R. Uecker, R. Bertram, M. Pietsch, A. Kwasniewski, M. Naumann, T. Schulz, R. Schewski, D. Klimm, M. Bickermann, On the bulk β-Ga2O3 single crystals grown by the Czochralski method, J. Cryst. Growth. 404 (2014) 184–191. https://doi.org/https://doi.org/10.1016/j.jcrysgro.2014.07.021.

[5] E.G. Víllora, K. Shimamura, Y. Yoshikawa, K. Aoki, N. Ichinose, Large-size β-Ga2O3 single crystals and wafers, J. Cryst. Growth. 270 (2004) 420–426. https://doi.org/https://doi.org/10.1016/j.jcrysgro.2004.06.027.

[6] E.G. Víllora, K. Shimamura, Y. Yoshikawa, T. Ujiie, K. Aoki, Electrical conductivity and carrier concentration control in β-Ga2O3 by Si doping, Appl. Phys. Lett. 92 (2008) 202120. https://doi.org/10.1063/1.2919728.

[7] J. Zhang, C. Xia, Q. Deng, W. Xu, H. Shi, F. Wu, J. Xu, Growth and characterization of new transparent conductive oxides single crystals β-Ga2O3: Sn, J. Phys. Chem. Solids. 67 (2006) 1656–1659. https://doi.org/https://doi.org/10.1016/j.jpcs.2006.02.018.

[8] N. Ma, N. Tanen, A. Verma, Z. Guo, T. Luo, H. (Grace) Xing, D. Jena, Intrinsic electron mobility limits in β-Ga2O3, Appl. Phys. Lett. 109 (2016) 212101. https://doi.org/10.1063/1.4968550.

[9] M. Yamaga, E.G. V\'\illora, K. Shimamura, N. Ichinose, M. Honda, Donor structure and electric transport mechanism in β−Ga2O3, Phys. Rev. B. 68 (2003) 155207.

https://doi.org/10.1103/PhysRevB.68.155207.

[10] J.F. Mcglone, Z. Xia, Y. Zhang, C. Joishi, S. Lodha, S. Rajan, S.A. Ringel, A.R. Arehart, Trapping Effects in Si δ -Doped β-Ga2O3 MESFETs on an Fe-Doped β-Ga2O3 Substrate, IEEE Electron Device Lett. 39 (2018) 1042–1045. https://doi.org/10.1109/LED.2018.2843344.

[11] M.E. Ingebrigtsen, A.Y. Kuznetsov, B.G. Svensson, G. Alfieri, A. Mihaila, U. Badstübner, A. Perron, L. Vines, J.B. Varley, Impact of proton irradiation on conductivity and deep level defects in β-Ga2O3, APL Mater. 7 (2018) 22510. https://doi.org/10.1063/1.5054826.

[12] K. Irmscher, Z. Galazka, M. Pietsch, R. Uecker, R. Fornari, Electrical properties of β-Ga2O3 single crystals grown by the Czochralski method, J. Appl. Phys. 110 (2011) 63720. https://doi.org/10.1063/1.3642962.

[13] Z. Zhang, E. Farzana, A.R. Arehart, S.A. Ringel, Deep level defects throughout the bandgap of (010) β-Ga 2 O 3 detected by optically and thermally stimulated defect spectroscopy, Appl. Phys. Lett. 108 (2016) 052105. https://doi.org/10.1063/1.4941429.

[14] A.Y. Polyakov, N.B. Smirnov, I. V Shchemerov, E.B. Yakimov, J. Yang, F. Ren, G. Yang, J. Kim, A. Kuramata, S.J. Pearton, Point defect induced degradation of electrical properties of Ga2O3 by 10 MeV proton damage, Appl. Phys. Lett. 112 (2018) 32107. https://doi.org/10.1063/1.5012993.

[15] A.Y. Polyakov, N.B. Smirnov, I. V Shchemerov, E.B. Yakimov, S.J. Pearton, C. Fares, J. Yang, F. Ren, J. Kim, P.B. Lagov, V.S. Stolbunov, A. Kochkova, Defects responsible for charge carrier removal and correlation with deep level introduction in irradiated β-Ga2O3, Appl. Phys. Lett. 113 (2018) 92102. https://doi.org/10.1063/1.5049130.

[16] J.B. Varley, J.R. Weber, A. Janotti, C.G. Van de Walle, Oxygen vacancies and donor impurities in β-Ga2O3, Appl. Phys. Lett. 97 (2010) 142106. https://doi.org/10.1063/1.3499306.

[17] J. Kim, S.J. Pearton, C. Fares, J. Yang, F. Ren, S. Kim, A.Y. Polyakov, Radiation damage effects in Ga2O3 materials and devices, J. Mater. Chem. C. 7 (2019) 10–24. https://doi.org/10.1039/C8TC04193H.

[18] J. Montes, C. Kopas, H. Chen, X. Huang, T. Yang, K. Fu, C. Yang, J. Zhou, X. Qi, H. Fu, Y. Zhao, Deep level transient spectroscopy investigation of ultra-wide bandgap (2̄01) and (001) β-Ga2O3, J. Appl. Phys. 128 (2020) 205701. https://doi.org/10.1063/5.0021859.

[19] R. Sun, Y.K. Ooi, A. Bhattacharyya, M. Saleh, S. Krishnamoorthy, K.G. Lynn, M.A. Scarpulla, Defect states and their electric field-enhanced electron thermal emission in heavily Zr-doped β -Ga 2 O 3 crystals, Appl. Phys. Lett. 117 (2020) 212104. https://doi.org/10.1063/5.0029442.

[20] S.R. Meitei, N.K. Singh, Post-deposition annealing effect on the structural, morphological, and photoluminescence properties of β-Ga2O3 nanowires deposited on silicon by glancing angle deposition, Appl. Phys. A. 125 (2019) 806. https://doi.org/10.1007/s00339-019-3075-x.

[21] H. Gao, S. Muralidharan, N. Pronin, M.R. Karim, S.M. White, T. Asel, G. Foster, S. Krishnamoorthy, S. Rajan, L.R. Cao, M. Higashiwaki, H. von Wenckstern, M. Grundmann, H. Zhao, D.C. Look, L.J. Brillson, Optical signatures of deep level defects in Ga2O3, Appl. Phys. Lett. 112 (2018) 242102. https://doi.org/10.1063/1.5026770.

[22] T. Dittrich, S. Fengler, N. Nickel, Surface Photovoltage Spectroscopy over Wide Time Domains for Semiconductors with Ultrawide Bandgap: Example of Gallium Oxide, Phys. Status Solidi. 218 (2021) 2100167. https://doi.org/https://doi.org/10.1002/pssa.202100167.

[23] H. Takane, K. Kaneko, T. Shinohe, S. Fujita, Analysis of Deep Traps in Mist Chemical Vapor Deposition-Grown n-Type α-Ga2O3 by Photocapacitance Method, Phys. Status Solidi. 258 (2021) 2000622. https://doi.org/https://doi.org/10.1002/pssb.202000622.

[24] A.Y. Polyakov, I.-H. Lee, N.B. Smirnov, E.B. Yakimov, I. V. Shchemerov, A. V. Chernykh, A.I. Kochkova, A.A. Vasilev, P.H. Carey, F. Ren, D.J. Smith, S.J. Pearton, Defects at the surface of β-Ga 2 O 3 produced by Ar plasma exposure, APL Mater. 7 (2019) 061102. https://doi.org/10.1063/1.5109025.

[25] E. Farzana, E. Ahmadi, J.S. Speck, A.R. Arehart, S.A. Ringel, Deep level defects in Ge-doped (010) β-Ga 2 O 3 layers grown by plasma-assisted molecular beam epitaxy, J. Appl. Phys. 123 (2018) 161410. https://doi.org/10.1063/1.5010608.

[26] A.R. Peaker, V.P. Markevich, J. Coutinho, Tutorial: Junction spectroscopy techniques and deep-level defects in semiconductors, J. Appl. Phys. 123 (2018) 161559. https://doi.org/10.1063/1.5011327.

[27] R. Roy, V.G. Hill, E.F. Osborn, Polymorphism of Ga2O3 and the System Ga2O3—H2O, J. Am. Chem. Soc. 74 (1952) 719–722. https://doi.org/10.1021/ja01123a039.

[28] M. Zinkevich, F. Aldinger, Thermodynamic Assessment of the Gallium-Oxygen System, J. Am. Ceram. Soc. 87 (2004) 683–691. https://doi.org/10.1111/j.1551-2916.2004.00683.x.

[29] S. Penner, C. Zhuo, R. Thalinger, M. Grünbacher, C. Hejny, S. Vanicek, M. Noisternig, Physico-chemical properties of unusual Ga2O3 polymorphs, Monatshefte Für Chemie - Chem. Mon. 147 (2016) 289–300. https://doi.org/10.1007/s00706-015-1628-z.

[30] H.Y. Playford, A.C. Hannon, E.R. Barney, R.I. Walton, Structures of Uncharacterised Polymorphs of Gallium Oxide from Total Neutron Diffraction, Chem. – A Eur. J. 19 (2013) 2803–2813. https://doi.org/10.1002/chem.201203359.

[31] S. Yoshioka, H. Hayashi, A. Kuwabara, F. Oba, K. Matsunaga, I. Tanaka, Structures and energetics of Ga 2 O 3 polymorphs, J. Phys. Condens. Matter. 19 (2007) 346211. https://doi.org/10.1088/0953-8984/19/34/346211.

[32] M. Bosi, P. Mazzolini, L. Seravalli, R. Fornari, Ga2O3 polymorphs: tailoring the epitaxial growth conditions, J. Mater. Chem. C. (2020). https://doi.org/10.1039/D0TC02743J.

[33] M.R. Delgado, C.O. Areán, Infrared Spectroscopic Studies on the Surface Chemistry of High-Surface-Area Gallia Polymorphs, Zeitschrift Für Anorg. Und Allg. Chemie. 631 (2005) 2115–2120. https://doi.org/10.1002/zaac.200570026.

[34] I. Cora, F. Mezzadri, F. Boschi, M. Bosi, M. Čaplovičová, G. Calestani, I. Dódony, B. Pécz, R. Fornari, The real structure of ε-Ga2O3 and its relation to κ-phase, CrystEngComm. 19 (2017) 1509–1516. https://doi.org/10.1039/C7CE00123A.

[35] M. Marezio, J.P. Remeika, Bond Lengths in the α-Ga2O3 Structure and the High-Pressure Phase of Ga2−xFexO3, J. Chem. Phys. 46 (1967) 1862–1865. https://doi.org/10.1063/1.1840945.

[36] S. Luan, L. Dong, R. Jia, Analysis of the structural, anisotropic elastic and electronic properties of β-Ga2O3 with various pressures, J. Cryst. Growth. 505 (2019) 74–81. https://doi.org/https://doi.org/10.1016/j.jcrysgro.2018.09.031.

[37] K. Pohl, Hydrothermale Bildung von γ-Ga2O3, Naturwissenschaften. 55 (1968) 82. https://doi.org/10.1007/BF00599490.

[38] H.Y. Playford, A.C. Hannon, M.G. Tucker, D.M. Dawson, S.E. Ashbrook, R.J. Kastiban, J. Sloan, R.I. Walton, Characterization of Structural Disorder in γ-Ga2O3, J. Phys. Chem. C. 118 (2014) 16188–16198. https://doi.org/10.1021/jp5033806.

[39] N.T. Son, K. Goto, K. Nomura, Q.T. Thieu, R. Togashi, H. Murakami, Y. Kumagai, A. Kuramata, M. Higashiwaki, A. Koukitu, S. Yamakoshi, B. Monemar, E. Janzén, Electronic properties of the residual donor in unintentionally doped β-Ga2O3, J. Appl. Phys. 120 (2016) 235703. https://doi.org/10.1063/1.4972040.

[40] J.P. McCandless, V. Protasenko, B.W. Morell, E. Steinbrunner, A.T. Neal, N. Tanen, Y. Cho, T.J. Asel, S. Mou, P. Vogt, H.G. Xing, D. Jena, Controlled Si doping of β-Ga2O3 by molecular beam epitaxy, Appl. Phys. Lett. 121 (2022) 72108. https://doi.org/10.1063/5.0101132.

[41] M.H. Wong, C.-H. Lin, A. Kuramata, S. Yamakoshi, H. Murakami, Y. Kumagai, M. Higashiwaki, Acceptor doping of β-Ga2O3 by Mg and N ion implantations, Appl. Phys. Lett. 113 (2018) 102103. https://doi.org/10.1063/1.5050040.

[42] F. Alema, G. Seryogin, A. Osinsky, A. Osinsky, Ge doping of β-Ga2O3 by MOCVD, APL Mater. 9 (2021) 91102. https://doi.org/10.1063/5.0059657.

[43] A. Parisini, A. Bosio, V. Montedoro, A. Gorreri, A. Lamperti, M. Bosi, G. Garulli, S. Vantaggio, R. Fornari, Si and Sn doping of ε-Ga2O3 layers, APL Mater. 7 (2019) 31114. https://doi.org/10.1063/1.5050982.

[44] W. Zhou, C. Xia, Q. Sai, H. Zhang, Controlling n-type conductivity of β-Ga2O3 by Nb doping, Appl. Phys. Lett. 111 (2017) 242103. https://doi.org/10.1063/1.4994263.

[45] Y. Shang, K. Tang, Z. Chen, Z. Zhang, J. Deng, Y. Hu, K. Gu, M. Cao, L. Wang, J. Huang, Growth and characterization of Ta-doped Ga2O3 films deposited by magnetron sputtering,

Mater. Sci. Semicond. Process. 134 (2021) 106040. https://doi.org/https://doi.org/10.1016/j.mssp.2021.106040.

[46] S. Bhandari, M.E. Zvanut, J.B. Varley, Optical absorption of Fe in doped Ga2O3, J. Appl. Phys. 126 (2019). https://doi.org/10.1063/1.5124825.

[47] I. López, E. Nogales, B. Méndez, J. Piqueras, A. Peche, J. Ramírez-Castellanos, J.M. González-Calbet, Influence of Sn and Cr Doping on Morphology and Luminescence of Thermally Grown Ga2O3 Nanowires, J. Phys. Chem. C. 117 (2013) 3036–3045. https://doi.org/10.1021/jp3093989.

[48] C.J. Zeman, S.M. Kielar, L.O. Jones, M.A. Mosquera, G.C. Schatz, Investigation of p-type doping in β- and κ-Ga2O3, J. Alloys Compd. 877 (2021) 160227. https://doi.org/10.1016/j.jallcom.2021.160227.

[49] C. Ma, Z. Wu, Z. Jiang, Y. Chen, W. Ruan, H. Zhang, H. Zhu, G. Zhang, J. Kang, T.-Y. Zhang, J. Chu, Z. Fang, Exploring the feasibility and conduction mechanisms of P-type nitrogen-doped β-Ga2O3 with high hole mobility, J. Mater. Chem. C. 10 (2022) 6673–6681. https://doi.org/10.1039/D1TC05324H.

[50] E. Chikoidze, C. Sartel, H. Mohamed, I. Madaci, T. Tchelidze, M. Modreanu, P. Vales-Castro, C. Rubio, C. Arnold, V. Sallet, Y. Dumont, A. Perez-Tomas, Enhancing the intrinsic p-type conductivity of the ultra-wide bandgap Ga2O3 semiconductor, J. Mater. Chem. C. 7 (2019) 10231–10239. https://doi.org/10.1039/c9tc02910a.

[51] T. Liu, Z. Feng, Q. Li, J. Yang, C. Li, M. Dupuis, Role of Oxygen Vacancies on Oxygen Evolution Reaction Activity: β-Ga2O3 as a Case Study, Chem. Mater. 30 (2018) 7714–7726. https://doi.org/10.1021/acs.chemmater.8b03015.

[52] L. Binet, D. Gourier, C. Minot, Relation between Electron Band Structure and Magnetic Bistability of Conduction Electrons in β-Ga2O3, J. Solid State Chem. 113 (1994) 420–433. https://doi.org/https://doi.org/10.1006/jssc.1994.1390.

[53] L. Dong, R. Jia, B. Xin, B. Peng, Y. Zhang, Effects of oxygen vacancies on the structural and optical properties of β-Ga2O3, Sci. Rep. 7 (2017) 40160. https://doi.org/10.1038/srep40160.

[54] A. Kyrtsos, M. Matsubara, E. Bellotti, Migration mechanisms and diffusion barriers of vacancies in Ga2O3, Phys. Rev. B. 95 (2017) 245202. https://doi.org/10.1103/PhysRevB.95.245202.

[55] M.D. McCluskey, Point defects in Ga2O3, J. Appl. Phys. 127 (2020) 101101. https://doi.org/10.1063/1.5142195.

[56] A. Usseinov, Z. Koishybayeva, A. Platonenko, V. Pankratov, Y. Suchikova, A. Akilbekov, M. Zdorovets, J. Purans, A.I. Popov, Vacancy Defects in Ga2O3: First-Principles Calculations of Electronic Structure, Materials (Basel). 14 (2021). https://doi.org/10.3390/ma14237384.

[57] G. Pozina, M. Forsberg, M.A. Kaliteevski, C. Hemmingsson, Emission properties of Ga2O3 nano-flakes: effect of excitation density, Sci. Rep. 7 (2017) 42132. https://doi.org/10.1038/srep42132.

[58] A.T. Neal, S. Mou, R. Lopez, J. V Li, D.B. Thomson, K.D. Chabak, G.H. Jessen, Incomplete Ionization of a 110 meV Unintentional Donor in β-Ga2O3 and its Effect on Power Devices, Sci. Rep. 7 (2017) 13218. https://doi.org/10.1038/s41598-017-13656-x.

[59] J.-N. Dang, S. Zheng, L. Chen, T. Zheng, Electronic structures and optical properties of Si- and Sn-doped β-Ga2O3: A GGA+U study*, Chinese Phys. B. 28 (2019) 16301. https://doi.org/10.1088/1674-1056/28/1/016301.

[60] D. Sun, Y. Gao, J. Xue, J. Zhao, Defect stability and electronic structure of doped β-Ga2O3: A comprehensive ab initio study, J. Alloys Compd. 794 (2019) 374–384. https://doi.org/https://doi.org/10.1016/j.jallcom.2019.04.253.

[61] M.E. Ingebrigtsen, J.B. Varley, A.Y. Kuznetsov, B.G. Svensson, G. Alfieri, A. Mihaila, U. Badstübner, L. Vines, Iron and intrinsic deep level states in Ga2O3, Appl. Phys. Lett. 112 (2018) 42104. https://doi.org/10.1063/1.5020134.

[62] S.M. Sze, K.K. Ng, Metal-Semiconductor Contacts, in: Phys. Semicond. Devices, John Wiley & Sons, Inc., Hoboken, NJ, USA, 2006: pp. 134–196. https://doi.org/10.1002/9780470068328.ch3.

[63] Z. Wang, X. Chen, F.-F. Ren, S. Gu, J. Ye, Deep-level defects in gallium oxide, J. Phys. D.

Appl. Phys. 54 (2021) 43002. https://doi.org/10.1088/1361-6463/abbeb1.

[64] L. Dobaczewski, I.D. Hawkins, A.R. Peaker, Laplace transform deep level transient spectroscopy: new insight into defect microscopy, Mater. Sci. Technol. 11 (1995) 1071–1073. https://doi.org/10.1179/mst.1995.11.10.1071.

[65] C. Zimmermann, Y.K. Frodason, A.W. Barnard, J.B. Varley, K. Irmscher, Z. Galazka, A. Karjalainen, W.E. Meyer, F.D. Auret, L. Vines, Ti- and Fe-related charge transition levels in β − Ga 2 O 3, Appl. Phys. Lett. 116 (2020) 72101. https://doi.org/10.1063/1.5139402.

[66] M.M. Islam, D. Rana, A. Hernandez, M. Haseman, F.A. Selim, Study of trap levels in β-Ga2O3 by thermoluminescence spectroscopy, J. Appl. Phys. 125 (2019) 55701. https://doi.org/10.1063/1.5066424.

[67] A.Y. Polyakov, N.B. Smirnov, I. V Shchemerov, S. V Chernykh, S. Oh, S.J. Pearton, F. Ren, A. Kochkova, J. Kim, Defect States Determining Dynamic Trapping-Detrapping in β-Ga2O3 Field-Effect Transistors, ECS J. Solid State Sci. Technol. 8 (2019) Q3013. https://doi.org/10.1149/2.0031907jss.

[68] A. Luchechko, V. Vasyltsiv, L. Kostyk, O. Tsvetkova, B. Pavlyk, The Effect of Cr3+ and Mg2+ Impurities on Thermoluminescence and Deep Traps in β-Ga2O3 Crystals, ECS J. Solid State Sci. Technol. 9 (2020) 45008. https://doi.org/10.1149/2162-8777/ab8b4d.

[69] C. Zimmermann, Y. Kalmann Frodason, V. Rønning, J.B. Varley, L. Vines, Combining steady-state photo-capacitance spectra with first-principles calculations: the case of Fe and Ti in β-Ga2O3, New J. Phys. 22 (2020) 63033. https://doi.org/10.1088/1367-2630/ab8e5b.

[70] Y. Ueda, T. Igarashi, K. Koshi, S. Yamakoshi, K. Sasaki, A. Kuramata, Two-inch Fe-doped β-Ga2O3 (010) substrates prepared using vertical Bridgman method, Jpn. J. Appl. Phys. 62 (2023) SF1006. https://doi.org/10.35848/1347-4065/acb55a.

[71] M. Higashiwaki, K. Sasaki, T. Kamimura, M. Hoi Wong, D. Krishnamurthy, A. Kuramata, T. Masui, S. Yamakoshi, Depletion-mode Ga2O3 metal-oxide-semiconductor field-effect transistors on β-Ga2O3 (010) substrates and temperature dependence of their device characteristics, Appl. Phys. Lett. 103 (2013) 123511. https://doi.org/10.1063/1.4821858.

[72] A.Y. Polyakov, I.H. Lee, N.B. Smirnov, E.B. Yakimov, I. V. Shchemerov, A. V. Chernykh,

A.I. Kochkova, A.A. Vasilev, P.H. Carey, F. Ren, D.J. Smith, S.J. Pearton, Defects at the surface of β -Ga2O3 produced by Ar plasma exposure, APL Mater. 7 (2019). https://doi.org/10.1063/1.5109025.

[73] C. Zimmermann, E. Førdestrøm Verhoeven, Y. Kalmann Frodason, P.M. Weiser, J.B. Varley, L. Vines, Formation and control of the center in implanted β-GaO by reverse-bias and zero-bias annealing, J. Phys. D. Appl. Phys. 53 (2020) 464001. https://doi.org/10.1088/1361-6463/aba64d.

[74] S. Bhandari, J.L. Lyons, D. Wickramaratne, M.E. Zvanut, Optical transitions of neutral Mg in Mg-doped β-Ga2O3, APL Mater. 10 (2022) 21103. https://doi.org/10.1063/5.0081925.

[75] S. Fujihara, Y. Shibata, Luminescence of Cr3+ ions associated with surpassing the green-emissive defect centers in β-Ga2O3, J. Lumin. 121 (2006) 470–474. https://doi.org/https://doi.org/10.1016/j.jlumin.2005.11.014.

[76] A.Y. Polyakov, A.I. Kochkova, A. Langørgen, L. Vines, A. Vasilev, I. V Shchemerov, A.A. Romanov, S.J. Pearton, On the possible nature of deep centers in Ga2O3, J. Vac. Sci. Technol. A. 41 (2023) 23401. https://doi.org/10.1116/6.0002307.

[77] J. Montes, C. Kopas, H. Chen, X. Huang, T. Yang, K. Fu, C. Yang, J. Zhou, X. Qi, H. Fu, Y. Zhao, Deep level transient spectroscopy investigation of ultra-wide bandgap (2̄01) and (001) β -Ga 2 O 3, J. Appl. Phys. 128 (2020) 205701. https://doi.org/10.1063/5.0021859.

[78] H. Ghadi, J.F. McGlone, C.M. Jackson, E. Farzana, Z. Feng, A.F.M.A.U. Bhuiyan, H. Zhao, A.R. Arehart, S.A. Ringel, Full bandgap defect state characterization of β-Ga2O3 grown by metal organic chemical vapor deposition, APL Mater. 8 (2020) 21111. https://doi.org/10.1063/1.5142313.

[79] K. Irmscher, Z. Galazka, M. Pietsch, R. Uecker, R. Fornari, Electrical properties of β -Ga 2 O 3 single crystals grown by the Czochralski method, J. Appl. Phys. 110 (2011) 063720. https://doi.org/10.1063/1.3642962.

[80] B.E. Kananen, L.E. Halliburton, K.T. Stevens, G.K. Foundos, N.C. Giles, Gallium vacancies in β-Ga2O3 crystals, Appl. Phys. Lett. 110 (2017) 202104. https://doi.org/10.1063/1.4983814.

[81] A.Y. Polyakov, N.B. Smirnov, I. V Shchemerov, S.J. Pearton, F. Ren, A. V Chernykh, P.B. Lagov, T. V Kulevoy, Hole traps and persistent photocapacitance in proton irradiated β-Ga2O3 films doped with Si, APL Mater. 6 (2018) 96102. https://doi.org/10.1063/1.5042646.

[82] J.B. Varley, A. Janotti, C. Franchini, C.G. de Walle, Role of self-trapping in luminescence and p-type conductivity of wide-band-gap oxides, Phys. Rev. B. 85 (2012) 81109. https://doi.org/10.1103/PhysRevB.85.081109.

[83] Z. Wang, H. Gong, C. Meng, X. Yu, X. Sun, C. Zhang, X. Ji, F. Ren, S. Gu, Y. Zheng, R. Zhang, J. Ye, Majority and Minority Carrier Traps in NiO/β-Ga 2 O 3 p + -n Heterojunction Diode, IEEE Trans. Electron Devices. 69 (2022) 981–987. https://doi.org/10.1109/TED.2022.3143491.

Graphical abstract:

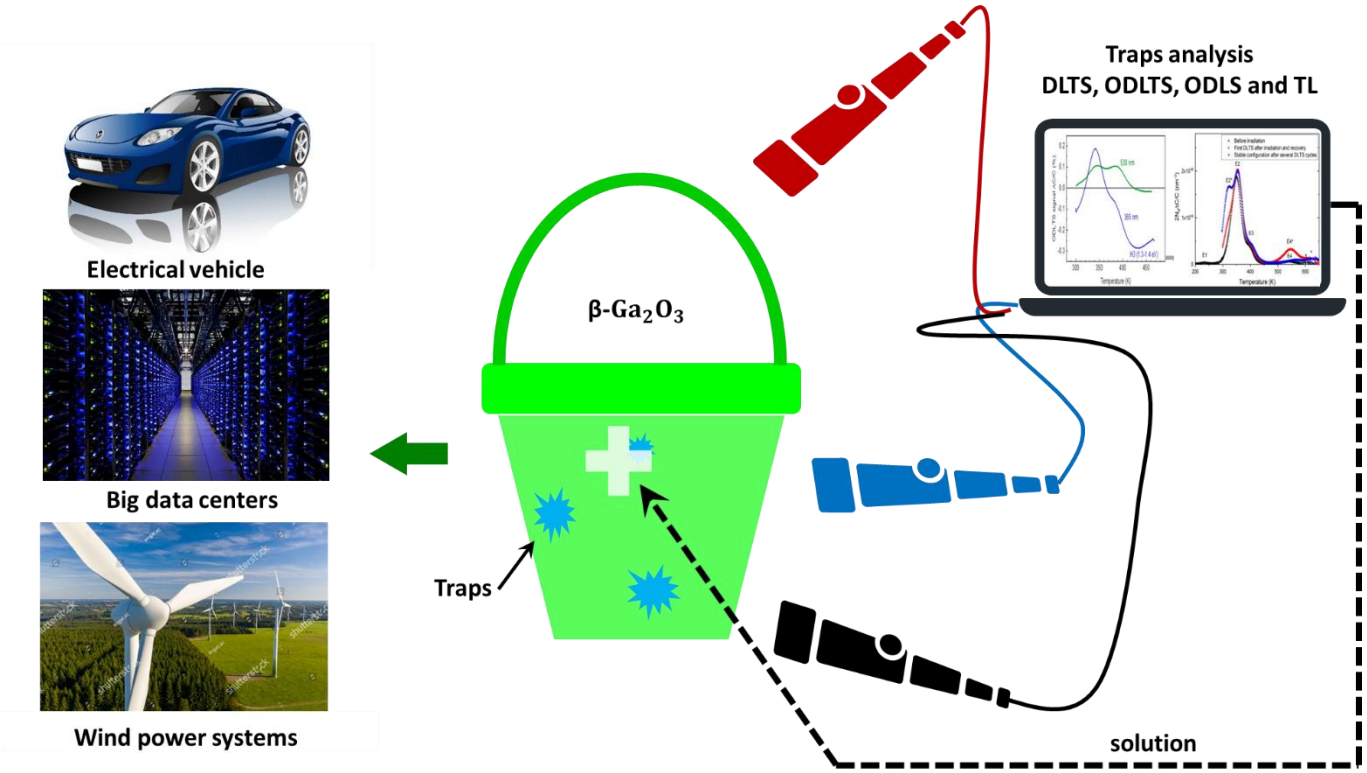

Tables list:

Table 1. Ga_2O_3 polymorphs and crystal structures.

Polymorph	System	Lattice parameters (Å)	Ref
α	Hexagonal	a=4.9825 b=13.433	[35]
β	Monoclinic	a=12.48 b=3.09 c=5.89 β=103.71	[36]
γ	Cubic	a=8.22	[37,38]
δ	Cubic	a=9.491	[31]
ε	Orthorhombic	a=5-5.1 b=8.7-8.8 c=9.2-9.4	[27]
κ	Orthorhombic	a=5.0463 b=8.7020 c=9.2833	[34]

Figures captions:

Figure 1: The crystal structures of monoclinic β-Ga_2O_3. The Ga and O atoms are represented by green and red spheres, respectively[36]. Reproduced with permission of J. Cryst. Growth. Copyright 2019 Elsevier.

Figure 2: β-Ga_2O_3 band structure shows a flat valence band[16]. Reproduced with permission of Appl. Phys. Lett. Copyright 2010 AIP Publishing.

Figure 3: Schematic representation of the unit cell of β-Ga_2O_3 with two nonequivalent Ga sites marked by small spheres Ga (I) (brown) and Ga (II) (orange). There are three nonequivalent O sites marked by big spheres O (I) (blue), O (II) (green) and O (III) (turquoise)[57]. Reproduced with permission of Sci. Rep. Copyright 2017 Springer Nature Publishing.

Figure 4: Formation energy versus Fermi level for several expected shallow donor impurities in β-Ga_2O_3 under (a) O-rich and (b) O-poor conditions[16]. Reproduced with permission of Appl. Phys. Lett. Copyright 2010 AIP Publishing.

Figure 5: Formation energy diagram for Fe in β-Ga_2O_3 shown for both Ga-rich and O-rich growth conditions. Ga (I) and Ga (II) denote two possible configurations of Ga in the lattice[61]. Reproduced with permission of Appl. Phys. Lett. Copyright 2018 AIP Publishing.

Figure 6: Energy band diagrams of a Schottky diode illustrating the occupancy changes at (a) $V=V_R$, (b) filling pulse $V=V_P$, and (c) thermal emission of electrons at $V=V_R$.

Figure 7: (a) DLTS signal at different temperatures of a β-Ga_2O_3 SBD. **(b)** Arrhenius plots of the deep trap levels[12]. Reproduced with permission of Appl. Phys J. Copyright 2011 AIP Publishing.

Figure 8: (a) DLTS spectra for β-Ga_2O_3 crystal and **(b)** the Arrhenius plots for three defects signatures. The inset shows the emission rate spectrum obtained from LDTS signal at 400 K[65]. Reproduced with permission of Appl. Phys J. Copyright 2020 AIP Publishing.

Figure 9: A schematic diagram of TL process[66]. Reproduced with permission of Appl. Phys. J. Copyright 2019 AIP Publishing.

Figure 10: DLTS traps detected before and after Ar plasma exposure. The length of the bars represents the relative concentrations[24]. Reproduced with permission of APL Mater. Copyright 2019 AIP Publishing.

Figure 11: DLTS measurements on bulk sample before and after Proton irradiation [11]. Reproduced with permission of APL Mater. Copyright 2018 AIP Publishing.

Figure 12: Energy diagram and trap levels in gallium oxide crystals: **(a)** unintentionally doped β-Ga_2O_3 (blue lines) and β-Ga_2O_3:0.05% Cr^{3+} (red lines); **(b)** β-Ga_2O_3:0.1%Mg^{2+} (green lines) and β-Ga_2O_3:0.05% Cr^{3+}, 0.1% Mg^{2+} (magenta lines)[68]. Reproduced with permission of ECS Journal of Solid State Science and Technology. Copyright 2020 IOP Publishing.

Figure 13: E2 concentration as measured by DLTS versus Fe^{+3} concentration (black squares) and Si concentration (red circles) as found by SIMS for bulk and epitaxial samples[61]. Reproduced with permission of Appl. Phys. Lett. Copyright 2018 AIP Publishing.

Figure 14: (a) DLTS spectra for-Ga_2O_3 deposited with different methods and **(b)** Comparison between the titanium concentration obtained from SIMS measurements and the trap concentration related to E3[65]. Reproduced with permission of Appl. Phys J. Copyright 2020 AIP Publishing.

Figure 15: Effect of neutron irradiation at different energy (a) 0.5 keV and (b) 5.0 keV[21]. Reproduced with permission of Appl. Phys. Lett. Copyright 2018 AIP Publishing.

Figure 16: ODLTS signal for Si-doped β-Ga_2O_3 with 365 nm LED excitation (blue line) and 530 nm LED excitation (olive line) [81]**.** Reproduced with permission of APL Mater. Copyright 2016 AIP Publishing.

Figure 17: (a) DLOS optical capture cross section and **(b)** its DLOS trap concentration [25]. Reproduced with permission of Appl. J. Appl. Phys. Copyright 2018 AIP Publishing.

Figure 18: Arrhenius plots for hole traps observed in ODLTS[81]. Reproduced with permission of APL Mater. APL Mater. Copyright 2016 AIP Publishing.

Figures list:

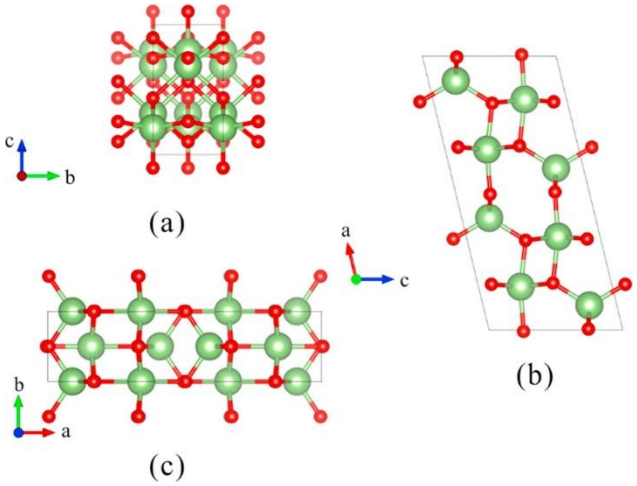

Figure 1: The crystal structures of monoclinic β-Ga_2O_3. The Ga and O atoms are represented by green and red spheres, respectively[36]. Reproduced with permission of J. Cryst. Growth. Copyright 2019 Elsevier.

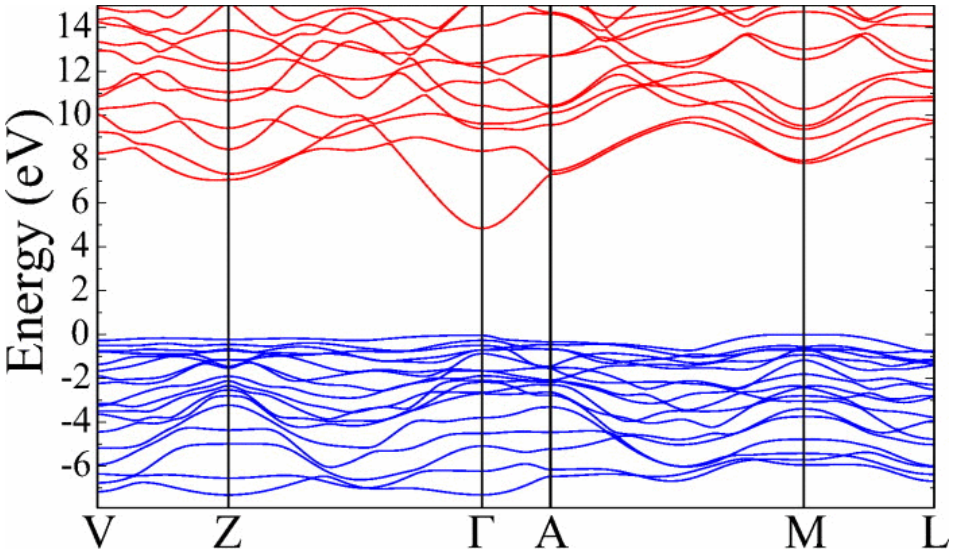

Figure 2: β-Ga_2O_3 band structure shows a flat valence band[16]. Reproduced with permission of Appl. Phys. Lett. Copyright 2010 AIP Publishing.

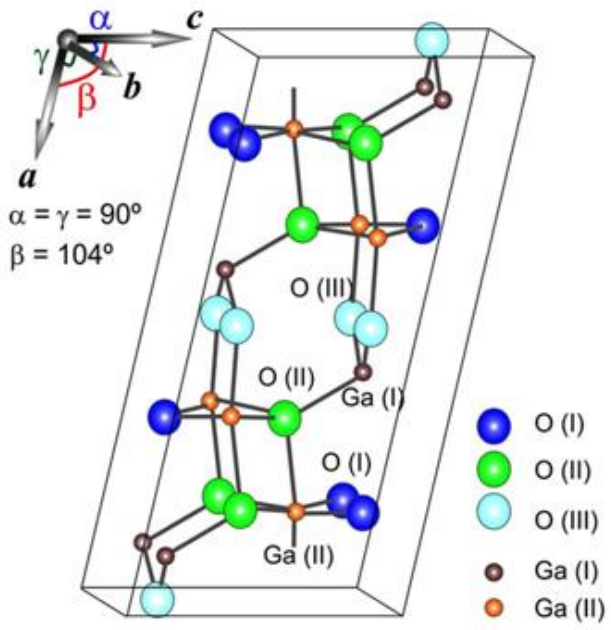

Figure 3: Schematic representation of the unit cell of β-Ga_2O_3 with two nonequivalent Ga sites marked by small spheres Ga (I) (brown) and Ga (II) (orange). There are three nonequivalent O

sites marked by big spheres O (I) (blue), O (II) (green) and O (III) (turquoise)[57]. Reproduced with permission of Sci. Rep. Copyright 2017 Springer Nature Publishing.

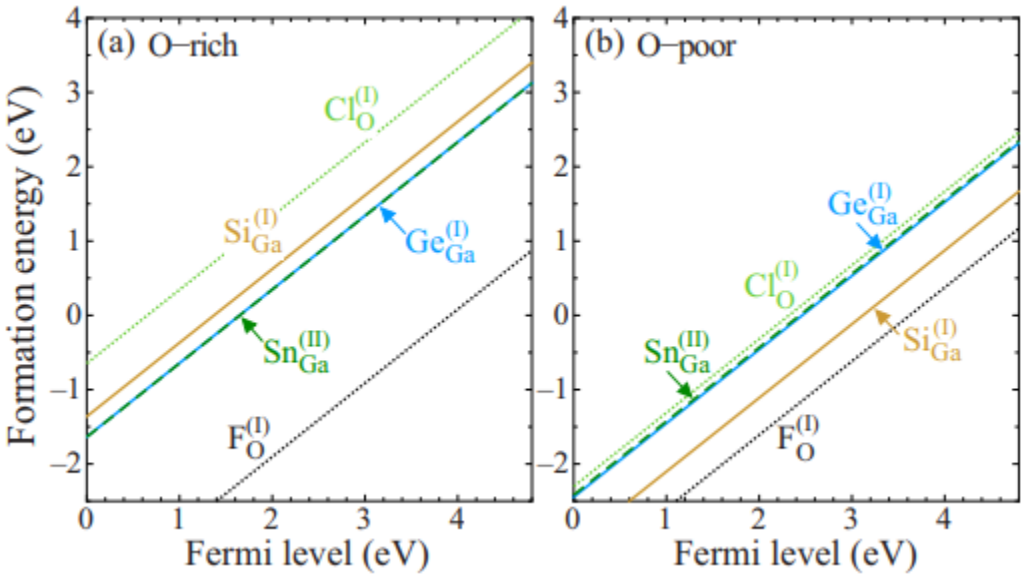

Figure 4: Formation energy versus Fermi level for several expected shallow donor impurities in β-Ga_2O_3 under (a) O-rich and (b) O-poor conditions[16]. Reproduced with permission of Appl. Phys. Lett. Copyright 2010 AIP Publishing.

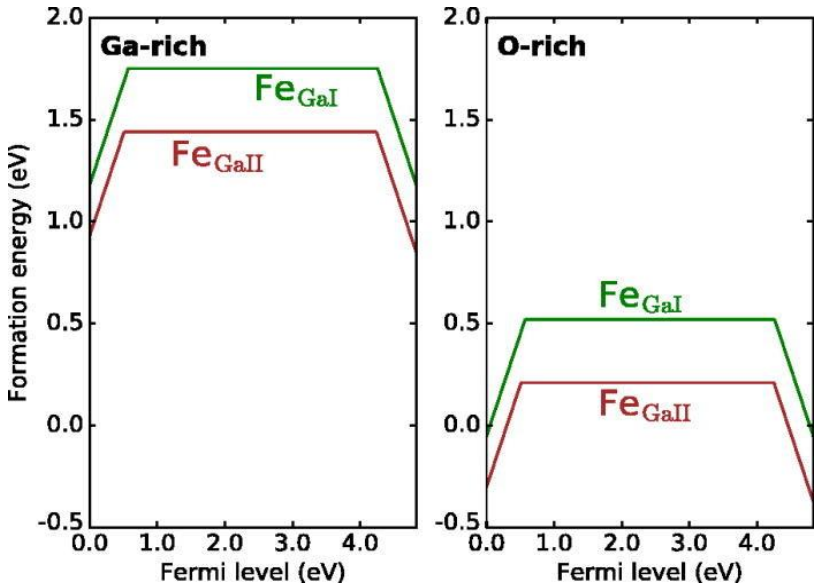

Figure 5: Formation energy diagram for Fe in β-Ga_2O_3 shown for both Ga-rich and O-rich growth conditions. Ga (I) and Ga (II) denote two possible configurations of Ga in the lattice[61]. Reproduced with permission of Appl. Phys. Lett. Copyright 2018 AIP Publishing.

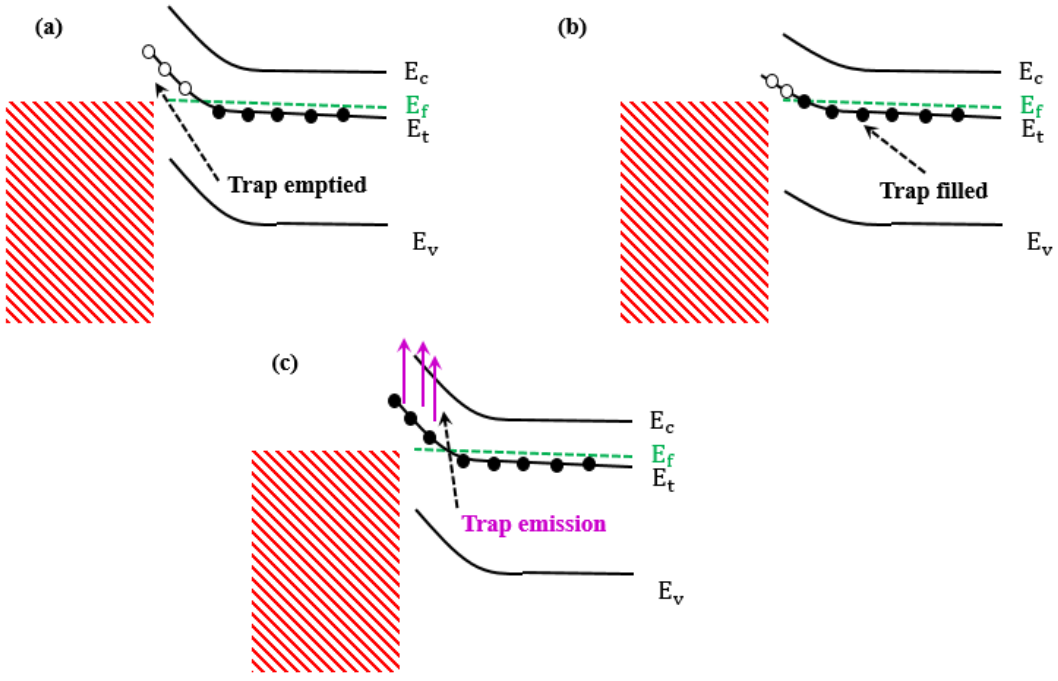

Figure 6: Energy band diagrams of a Schottky diode illustrating the occupancy changes at (a) $V=V_R$, (b) filling pulse $V=V_P$, and (c) thermal emission of electrons at $V=V_R$.

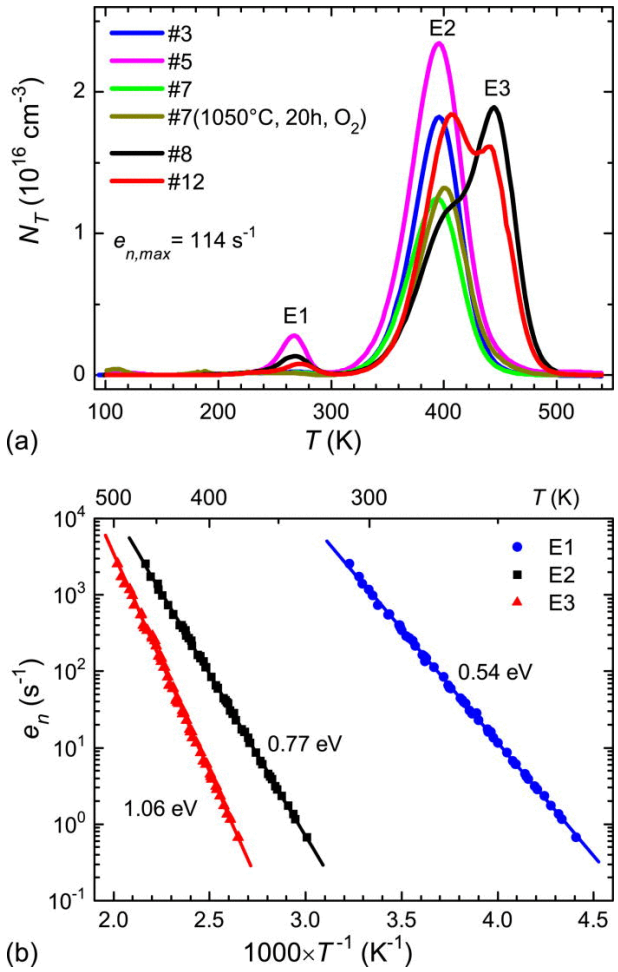

Figure 7: (a) DLTS signal at different temperatures of a β-Ga_2O_3 SBD. **(b)** Arrhenius plots of the deep trap levels[12]. Reproduced with permission of Appl. Phys J. Copyright 2011 AIP Publishing.

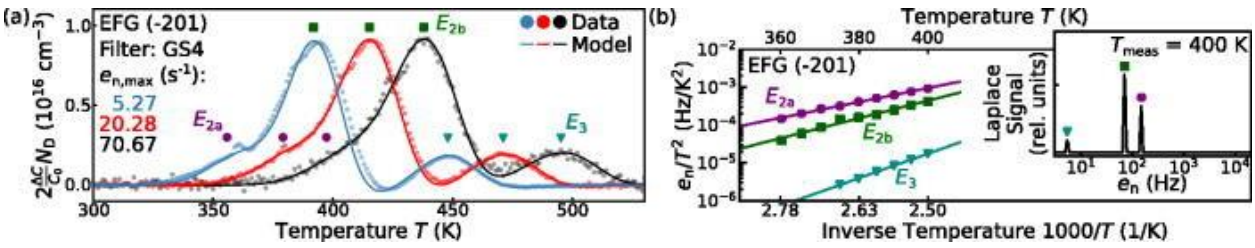

Figure 8: (a) DLTS spectra for β-Ga_2O_3 crystal and **(b)** the Arrhenius plots for three defects signatures. The inset shows the emission rate spectrum obtained from LDTS signal at 400 K[65]. Reproduced with permission of Appl. Phys J. Copyright 2020 AIP Publishing.

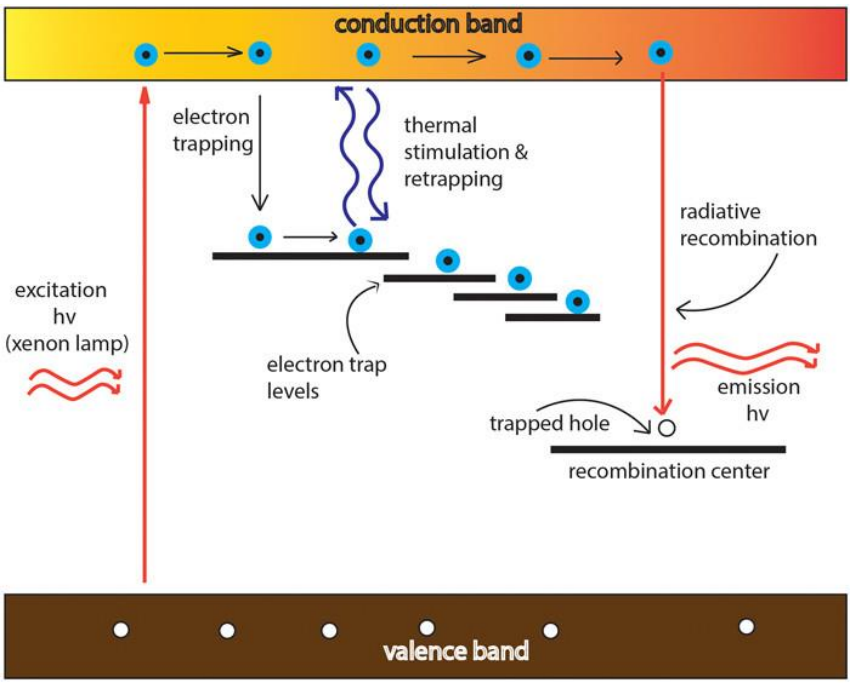

Figure 9: A schematic diagram of TL process[66]. Reproduced with permission of Appl. Phys. J. Copyright 2019 AIP Publishing.

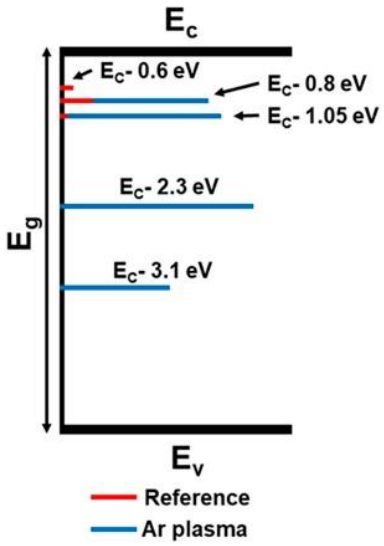

Figure 10: DLTS traps detected before and after Ar plasma exposure. The length of the bars represents the relative concentrations[24]. Reproduced with permission of APL Mater. Copyright 2019 AIP Publishing.

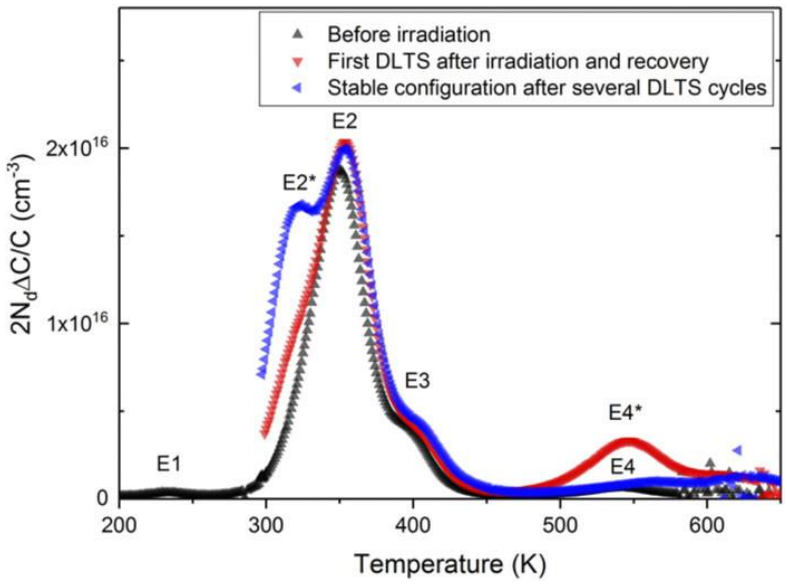

Figure 11: DLTS measurements on bulk sample before and after Proton irradiation [11]. Reproduced with permission of APL Mater. Copyright 2018 AIP Publishing.

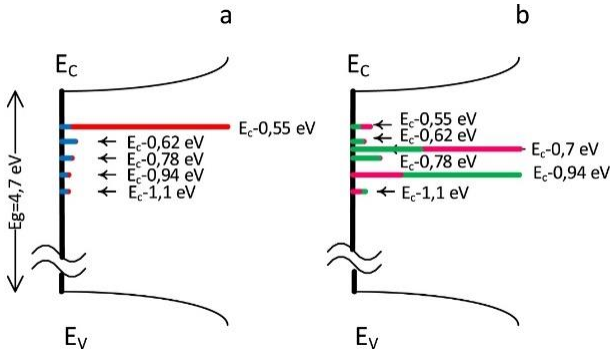

Figure 12: Energy diagram and trap levels in gallium oxide crystals: **(a)** unintentionally doped β-Ga_2O_3 (blue lines) and β-Ga_2O_3:0.05% Cr^{3+} (red lines); **(b)** β-Ga_2O_3:0.1%Mg^{2+} (green lines) and β-Ga_2O_3:0.05% Cr^{3+}, 0.1% Mg^{2+} (magenta lines)[68]. Reproduced with permission of ECS Journal of Solid State Science and Technology. Copyright 2020 IOP Publishing.

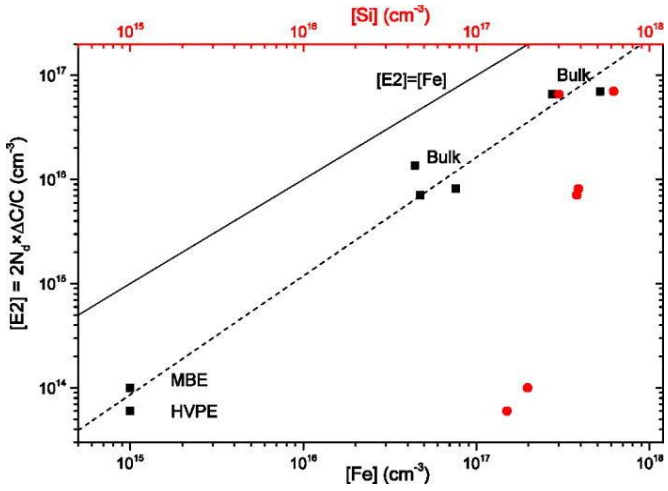

Figure 13: E2 concentration as measured by DLTS versus Fe^{+3} concentration (black squares) and Si concentration (red circles) as found by SIMS for bulk and epitaxial samples[61]. Reproduced with permission of Appl. Phys. Lett. Copyright 2018 AIP Publishing.

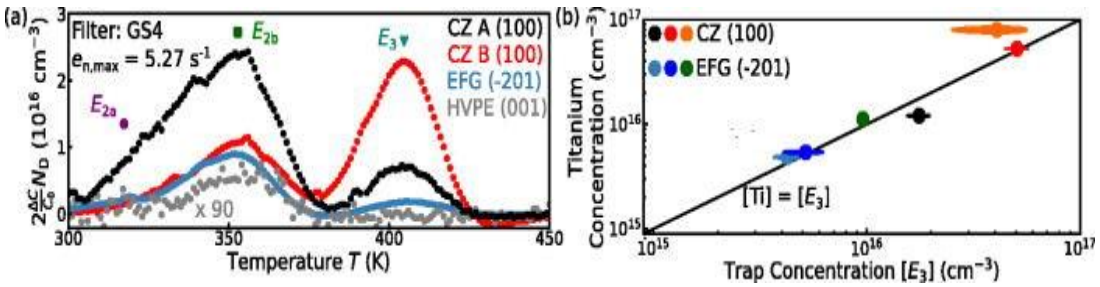

Figure 14: (a) DLTS spectra for-Ga_2O_3 deposited with different methods and **(b)** Comparison between the titanium concentration obtained from SIMS measurements and the trap concentration related to E3[65]. Reproduced with permission of Appl. Phys J. Copyright 2020 AIP Publishing.

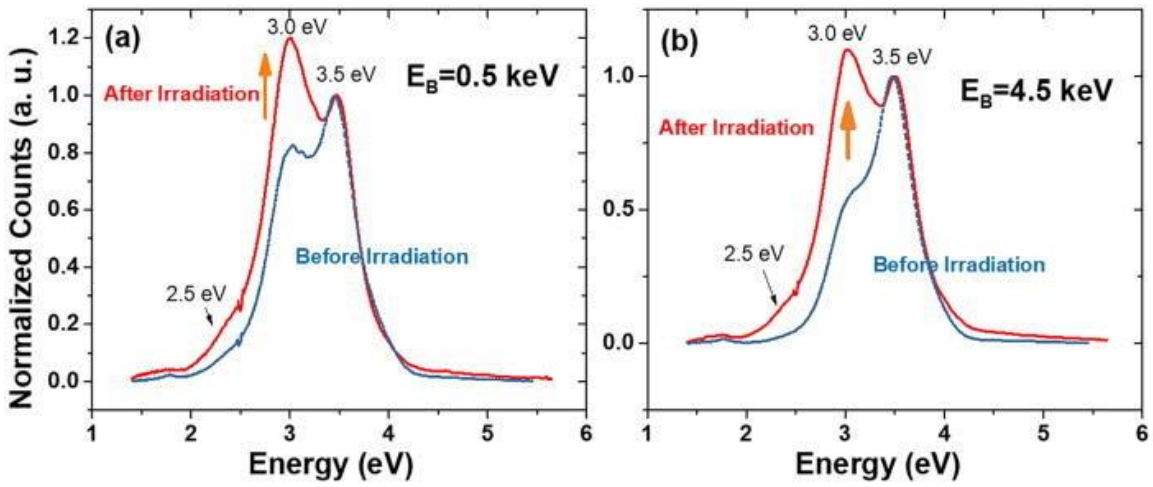

Figure 15: Effect of neutron irradiation at different energy (a) 0.5 keV and (b) 5.0 keV[21]. Reproduced with permission of Appl. Phys. Lett. Copyright 2018 AIP Publishing.

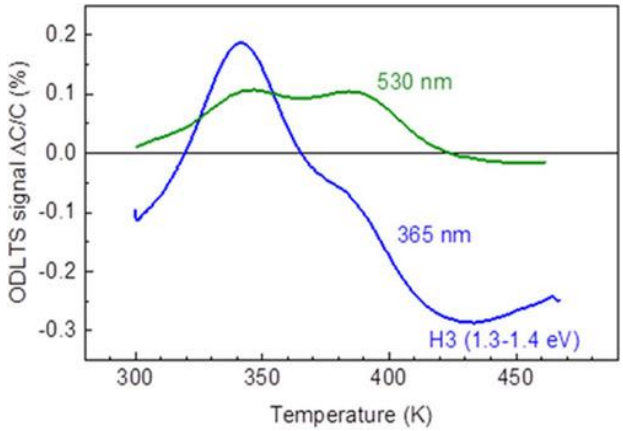

Figure 16: ODLTS signal for Si-doped β-Ga_2O_3 with 365 nm LED excitation (blue line) and 530 nm LED excitation (olive line) [81]**.** Reproduced with permission of APL Mater. Copyright 2016 AIP Publishing.

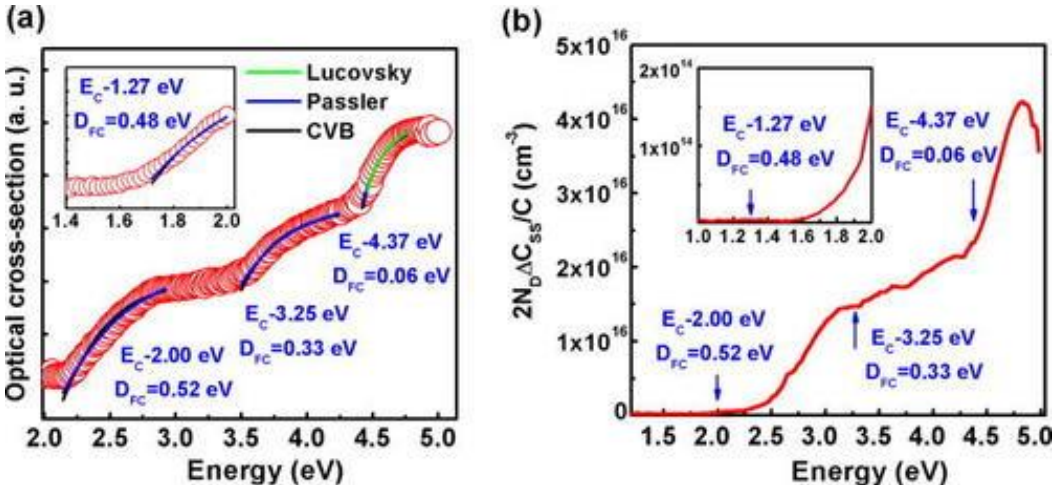

Figure 17: (a) DLOS optical capture cross section and **(b)** its DLOS trap concentration [25]. Reproduced with permission of Appl. J. Appl. Phys. Copyright 2018 AIP Publishing.

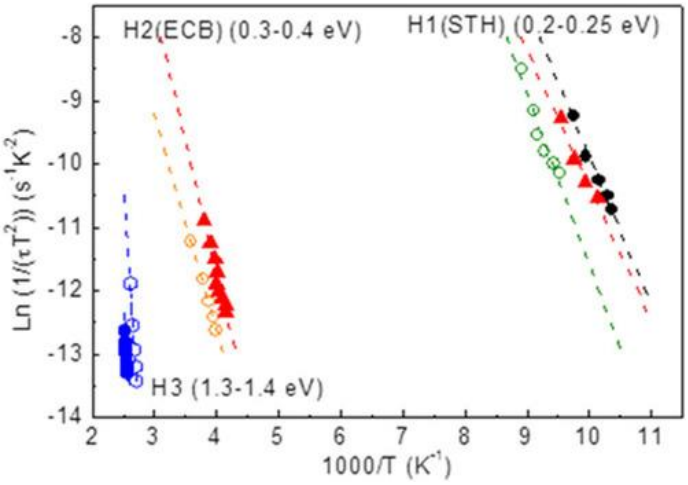

Figure 18: Arrhenius plots for hole traps observed in ODLTS[81]. Reproduced with permission of APL Mater. APL Mater. Copyright 2016 AIP Publishing.